THE JOURNAL OF PHYSICAL CHEMISTRY C

pubs.acs.org/JPCC Article

Formic Acid Synthesis in a Water–Mineral System: Major Role of the Interface

Sara Laporte,* Fabio Pietrucci, François Guyot, and A. Marco Saitta

Cite This: J. Phys. Chem. C 2020, 124, 5125–5131 Read Online

ACCESS | Metrics & More | Article Recommendations | Supporting Information

ABSTRACT: Mineral surfaces are known for their catalytic properties, as they have lower kinetic barriers to reactions and modify chemical equilibria. Using ab initio molecular dynamics and enhanced sampling methods, we predict that the MgO(001)–water interface thermodynamically favors the formation of formic acid from carbon monoxide and water. This occurs despite the lack of direct participation from the surface atoms, with the reaction taking place beyond the first adsorbed layer. Furthermore, the application of an external electric field on the reaction in bulk water shows a similar effect. We propose that formic acid may be stabilized by the surface electric field, by direct comparison with the equilibrium in bulk water with and without an external electric field applied, and at the MgO(001)–water interface.

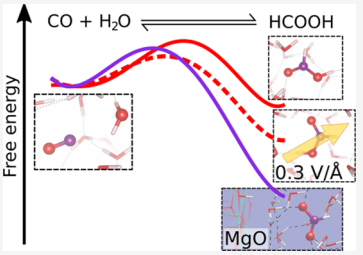

INTRODUCTION

Reactions involving formic acid have been widely studied due to their potential use for energy conversion and storage, as well as their industrial and geochemical relevance. Formic acid is a known intermediate state in the water–gas shift reaction, making it a possible alternative to hydrogen as a clean fuel.[1] In the agricultural sector, use of formic acid has increased as an antibacterial agent, following bans on antibiotics as growth promoters, all-in-all resulting in an estimated worldwide production of 760 kt in 2019.[2,3] In prebiotic geochemistry, formic acid is a relevant precursor, along with formamide and hydrogen cyanide, to both amino acids and sugars.[4] The reversible decomposition of formic acid is known to occur through two competing pathways, which may be tuned according to pressure and temperature,[5] concentration in aqueous solution,[6] and the choice of the substrate when the reaction is surface-catalyzed.[7] Under hydrothermal conditions and at low concentrations of formic acid, CO_2 has been found to be the main decomposition product,[6] whereas CO is the main product at higher concentrations and lower temperatures.[1,6,8] This case also presents an interesting problem as water plays the triple role of a solvent, a reactant, and a catalyst. In this work, we simulate the synthesis of formic acid from carbon monoxide and water (eq 1) at 400 K with 1 g/cm^3 density and 1.6 M concentration (corresponding to one formic acid molecule per box). Some simulations were also run at 300 K at the same density and concentration, and these are included in the Supporting Information. In this regime, the expected reversible decomposition pathway (from right to left in eq 1) is referred to in the literature as decarbonylation or dehydration, as follows

$$CO + H_2O \rightleftharpoons HCOOH \quad (1)$$

Various factors may shift the thermodynamics of the reaction, favoring either the synthesis or the decomposition of formic acid.[1] In addition to changing the temperature and, to a lesser extent, density/pressure, such shifts may be induced by changing the solvent to an ionic liquid,[9] or in the vicinity of an oxide surface.[10] Both alumina (Al_2O_3)[11] and magnesia (MgO)[12,13] have been shown to catalyze this reaction in the gas phase, as do aluminosilicate zeolites;[14] however, due to the large computational cost, theoretical investigations to date have been limited to oxide surfaces in a vacuum.[15] Nevertheless, the mineral–water interface might have a significant effect on the thermodynamics and kinetics of the reaction, not only due to the specific catalytic effect of the atoms making up the surface but also due to the modified dielectric and acid–basic environment in the interfacial water. In fact, water, at mineral or indeed even at soft-matter interfaces,[16] tends to exhibit particular properties due to its confinement. The electric double layer (EDL) at the mineral–water interfaces has been extensively studied, and in many cases, there exists a dense layer of water at the interface,[17,18] with the water molecules oriented according to the the surface charge.[19] The EDL is characterized by a short-range but intense electric field on the order of V/Å.[20,21] This is comparable to electric fields generated at the catalytic sites of enzymes.[22] Both at clay surfaces[23] and in planar confinement between polar membranes,[16] the dielectric constant of water within a few angstroms of the surface has been shown to decrease dramatically, thus enhancing electrostatic interactions. Water near the surface is not only confined but also exhibits electrostatic properties that differ greatly from those of the bulk. Electric fields have also been shown to greatly impact the

Received: October 23, 2019
Revised: February 11, 2020
Published: February 12, 2020

reaction pathways and free energy landscapes in geochemical contexts.[24,25] Thus, in this study, we compare the decarbonylation reaction in three distinct cases: in bulk water, in bulk water with an electric field applied, and at the MgO(001)−water interface, characterized in previous work.[21] In the case where a homogeneous electric field is applied, the intensity was chosen at 0.3 V/Å, just below the dissociation threshold of water.[26,27] Due to the small size and short time scales of the simulations, we do not consider longer-scale equilibria such as the potentially irreversible alterations in the mineral surface. We present ab initio molecular dynamics simulations combined with state-of-the-art enhanced sampling approaches[4,28] to reconstruct the mechanisms and quantitative free-energy profiles for the chemical reaction of interconverting carbon monoxide and formic acid. Although reactions involving formic acid have been previously studied by ab initio means,[29−31] the solvent had not yet been taken into account explicitly, and no attempt has been made in previous studies to involve interfacial water at a mineral surface. The application of an external electric field to this reaction network is also completely novel.

COMPUTATIONAL DETAILS

All simulations are density functional theory (DFT)-based molecular dynamics (MD), as implemented in the code Quantum ESPRESSO,[33] employing the Perdew−Burke−Ernzerhof (PBE) functional[32] including the Grimme correction term[33,34] to take into account dispersion interactions. We adopted the Car−Parrinello scheme[35] for bulk water simulations, taking advantage of the efficient Berry phase implementation of external homogeneous electric fields;[36] Born−Oppenheimer MD was employed for simulations at the mineral−water interface. The temperature was controlled using stochastic velocity rescaling.[37] Simulations presented here were all run at 400 K, but some results at 300 K are also presented in the Supporting Information. The bulk liquid models consist of periodically repeated cubic supercells of side 10.051 Å, initially including 34 water molecules and one carbon monoxide molecule, corresponding to a density of 1 g/cm^3. The supercells used to simulate the surface consists of six layers of cubic MgO (periclase), 24 atoms each, arranged in a slab geometry in the (001) direction (here called the z-direction) in contact with liquid water. The x- and y-dimensions of the box are commensurate with the known (2 × 3) reconstruction of the first adsorbed layer of water on MgO(001),[21] while the z-dimension was chosen by setting the average density between the slabs as 1 g/cm^3, resulting in dimensions of 11.94 × 8.94 × 30.37 Å^3. Between the slabs are present a total of 66 water molecules and 2 carbon monoxide molecules. This is the equivalent of six layers of water, with one strongly adsorbed and partly dissociated layer, followed by a region in which the radial distribution function (RDF) between water molecules is almost indistinguishable from the bulk RDF, despite the small box size.[21] The CO molecules were initially placed just beyond the first adsorbed water layer (one on each side) and were not found to diffuse away from their respective surfaces, without the need for constraints, throughout unbiased simulations of 6 ps. The reaction was accelerated applying metadynamics[38] only on one of the two CO molecules, leaving the other one unbiased. An equilibrium trajectory was also generated on the box with formic acid on one side and CO on the other: a corresponding snapshot is shown in Figure 1a, along with the distribution of each atomic species along the z-axis in the unbiased cases (Figure 1b,c).

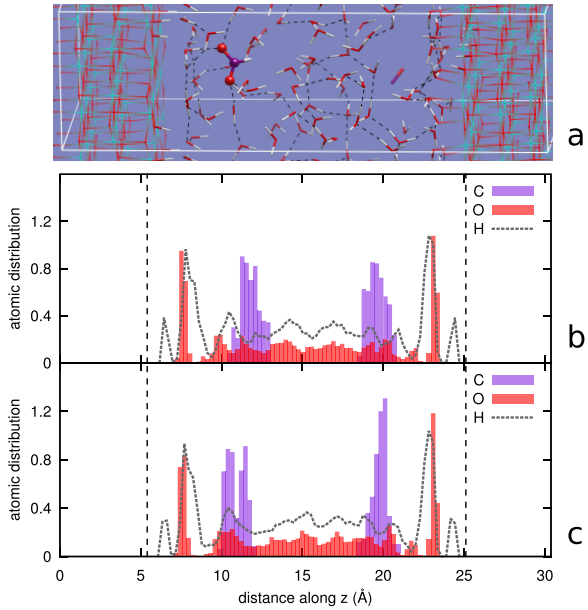

Figure 1. (a) Snapshot of the simulation box while formic acid is formed at the MgO−water interface. (b) Distribution of each atomic species in the unbiased run with only solvated CO at the MgO−water interface. (c) Distribution of each atomic species during the unbiased run, with formic acid on the left side of the box and CO on the right side. In each case, the relative counts for C are multiplied for visibility, whereas those for O and H are correctly normalized with respect to each other (two hydrogen atoms for each oxygen atom). The average position of the surface MgO atoms is shown as dotted vertical lines.

To obtain free energy profiles for the targeted reaction, a combination of enhanced sampling techniques,[4,28] namely, metadynamics[38] and umbrella sampling,[39] was used. We adopted the path coordinates as collective variables (CVs)[40] on the basis of the topological metric of ref 4. These CVs have been found to be highly effective for chemical reactions in solution,[41−45] tracking changes in chemical bond networks passing from reactants to products , through intermediate/transition states, while also enabling solvent participation. Furthermore, the specific definition of the two-dimensional path CV does not specify intermediate states but only reference states of reactants and products: the system is free to spontaneously discover a reaction path. Hydrogen atoms are not individually labeled to define reference states but taken into account as coordination numbers, so that protons can be freely exchanged with the solvent. Finally, as formic acid may exist in the cis or trans rotamer, or (after dissociation of the acidic proton) as the formate ion, our particular choice of CV is convenient because the three possible product species are near each other in the CV space, and the system was able to reach its preferred rotamer in all cases. A freely available, modified version of the Plumed 1.3 plugin was used[46] for metadynamics and umbrella sampling runs. The collective variable and simulation protocol used is described in more detail in the Supporting Information.

RESULTS AND DISCUSSION

Rotamer Selection. In bulk water, the cis rotamer of formic acid was formed in the absence of an electric field,

https://dx.doi.org/10.1021/acs.jpcc.9b09979
J. Phys. Chem. C 2020, 124, 5125−5131

whereas the trans rotamer was formed when an electric field was applied. In the case of surface, the trans rotamer was initially formed. Subsequently, unbiased simulations were run initially with the cis rotamer, and in both the electric field, and on the surface, the trans rotamer was quickly attained spontaneously through proton exchange with the solvent. Although *cis*-formic acid was stable in the simulation in bulk water with no field, the formate ion was synthesized when starting from the trans rotamer both in bulk water with an electric field and in the interfacial water after a proton transfer event. In the electric field, we were able to identify a dozen switching events in a 14 ps trajectory, each between 0.5 and 2 ps apart. On the surface, only two switching events between *trans*-HCOOH and formate took place during 6 ps. The tracking of the species type along the trajectory can be found in Figure 2. The definition of the ionization state of the molecules

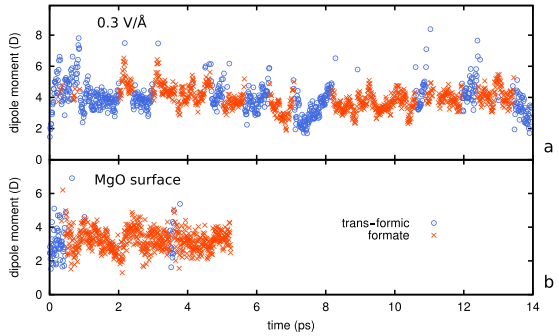

Figure 2. Tracking of the species type and dipole moment for the unbiased runs of the product in an electric field (a) and at the MgO–water interface (b).

here is based on a distance criterion, whereby each hydrogen atom was defined as uniquely "belonging" to its nearest neighbor carbon or oxygen atom. This definition, although somewhat simplistic, enables us to dynamically differentiate between hydroxide ions, water molecules, and hydronium ions, as centered on oxygen atoms "owning" exactly one, two, or three hydrogen atoms, respectively. In this way, we were also able to label formic acid differently from the formate ion, without the need to select an arbitrary cutoff distance.

Dipole Moments. In an attempt to explain the rotamer selection induced by the field and the surface, molecular dipole moments were calculated by means of maximally localized Wannier functions (MLWF).[47] Using these as representative charge centers for the valence electrons, represented as blue spheres in Figure 3, and atomic positions as positive charge centers, we were able to calculate the dipole moments of each molecule in solution. A dipole moment for $HCOO^-$ was also computed keeping in mind that for a charged molecule, this depends on the choice of origin, here chosen to be the center of mass of the molecule. This results in value comparable to that of the trans rotamer, and through the dynamics at proton transfer events, the computed dipole moment was found to be somewhat continuous, as shown in Figure 2, along with the histograms of the dipole moments in Figure 4. The dipole moment of CO in water is thus calculated to be 0.3 D. Its tabulated value in the gas phase is 0.122 D.[48]

For formic acid, tabulated values are about an order of magnitude larger than CO (1.4 D in the gas phase),[49] as also found here. For the cis rotamer, the dipole moment computed here averages at 7.5 D and can reach up to 10 D, while the trans rotamer shows dipole moments averaging between 3 and 4 D. Values computed in ref 50, at the MP2 level of theory and in a polarizable continuum model, are 5.19 D for the cis rotamer and 1.93 D for the trans rotamer.

Experimental values of the dipole moment of carbon monoxide and formic acid in water were not found in the literature; however, we expect solvation to increase the dipole moment, as it does for example for ethanol,[51] or for water itself.[52] Although calculated values of dipole moments for small molecules within DFT vary depending on the functional,[53] the large difference in dipole moments between the two rotamers might explain why the trans rotamer, more stable than cis in vacuum but not in water solution, is again more stable in the lowered dielectric environments that are water in an electric field[54] and the water–mineral interface.[16,55]

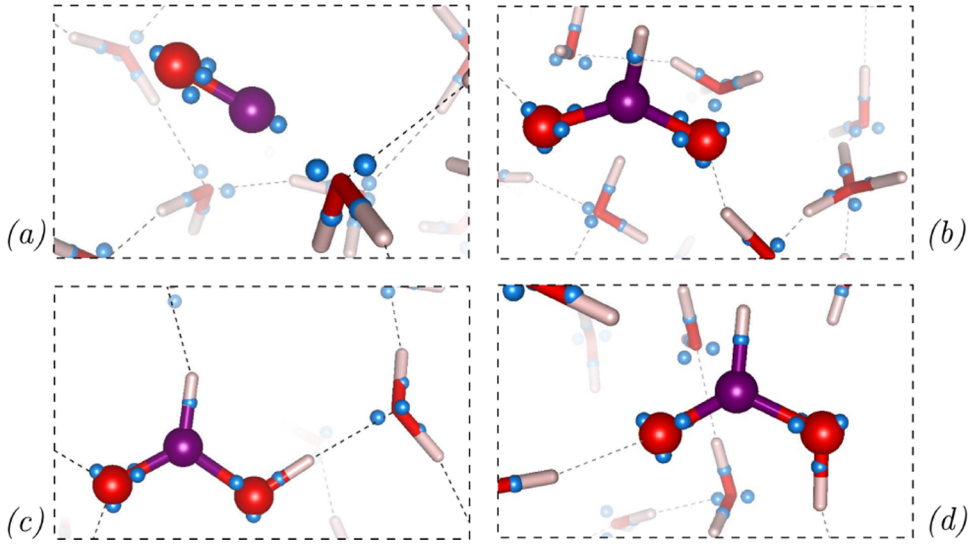

Figure 3. Snapshots of the simulations in bulk water. The top left shows carbon monoxide and water; the top right shows a solvated formate ion, with the hydronium ion visible in the solvent. The bottom panels show solvated formic acid, in the cis (left) and trans (right) configurations. Wannier centers that were used to compute dipole moments in solution are shown as light blue spheres.

https://dx.doi.org/10.1021/acs.jpcc.9b09979
J. Phys. Chem. C 2020, 124, 5125–5131

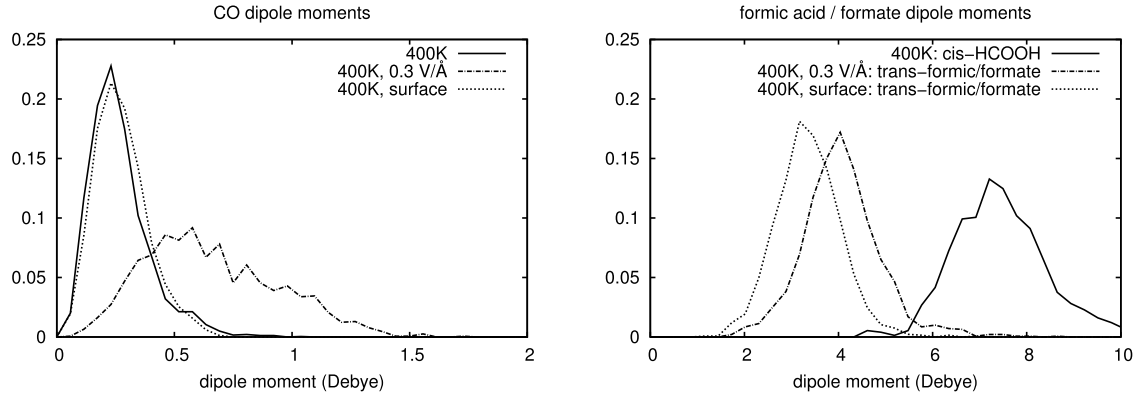

Figure 4. Histograms of the dipole values as calculated using Wannier centers. For formic acid, the distributions differ between the no field and field or surface cases due to the cis rotamer having a much larger dipole moment than the trans rotamer.

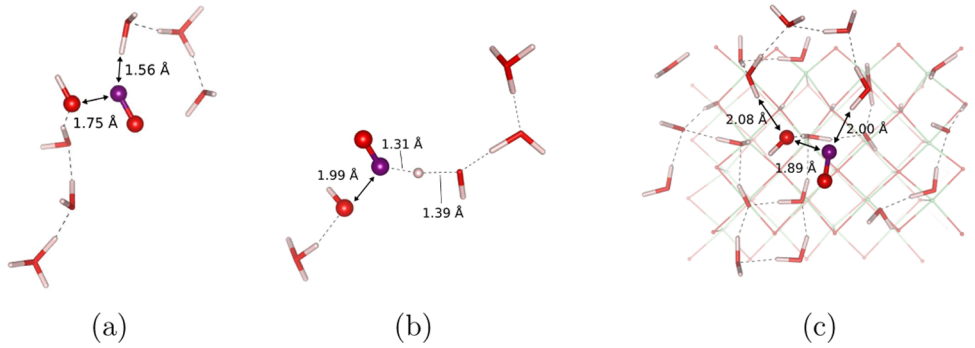

Figure 5. Transition states extracted from committor analysis MD trajectories at 400 K; in bulk solution without external electric field (a), with an applied electric field (b), and at the MgO−water interface (c). Only the water molecules involved in the reaction are shown, except in the surface case where the adsorbed water molecules are also shown.

Transition States. The selected rotamer in each case reflects the structure of the transition state for decarbonylation. The transition states observed during the exploratory metadynamics run at 400 K are shown in Figure 5. As shown in ref 6 in which transition states are calculated at the DFT-B3LYP level of theory in the gas phase, and intuitively from the structure of the transition state, the first geometry (Figure 5a) would lead to *cis*-HCOOH, while the second would lead to *trans*-HCOOH (Figure 5b,5c).

Free Energy Profiles. Free energy profiles were obtained in bulk water at 400 K, with and without an applied electric field, and at the MgO−water interface at 400 K as reported in Figure 6. Using block analysis on the umbrella sampling runs, we estimate the precision achieved with our protocol to be ±2 kcal/mol (details given in the Supporting Information). Formic acid is found to be 23 kcal/mol more stable than reactants upon applying an electric field, while it is 42 kcal/mol more stable than reactants at the interface with the mineral surface. This difference in the free energy of formic acid can be in part explained by the fact that a different rotamer is stabilized (cis in the bulk water case, trans in the electric field and at the interface). Furthermore, bulk water, water in an electric field, and water at an interface, each have distinct solvation properties, which have been shown to play a key role in shifting reaction equilibria, as for example in the case of formic acid solvated in an ionic liquid.[9]

Furthermore, this significant variation in the free energy landscape is surprising, considering it occurs without direct adsorption on the surface (see Figure 1). We may partly interpret this as the action of the surface electric field. From

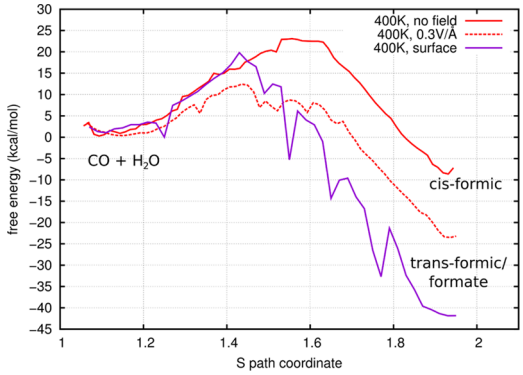

Figure 6. Comparison of free energy profiles for the reaction in solution with and without an electric field and at the MgO−water interface. The free energies of reactants are arbitrarily aligned.

our previous work on the MgO(001)−water interface, the intensity of the spontaneous local electric field where the reaction occurs, 4−6 Å from the surface atoms, is about 0.5 V/Å.[21] An indication of the analogous effect of mineral surface and an external electric field is given by the fact that both select the *trans*-HCOOH rotamer and both set to approximately zero the free energy difference between HCOOH and $HCOO^-$, with spontaneous easy interconversion between the two (see Figure 2 and the corresponding discussion).

As shown in Figure 6, the stabilization of the products with respect to reactants, as provoked by the applied electric field or the presence of the mineral surface, corresponds to the geometry of the transition state approaching the reactants

https://dx.doi.org/10.1021/acs.jpcc.9b09979
J. Phys. Chem. C 2020, 124, 5125−5131

Table 1. Comparison of the Values for the Equilibrium Constant, Free Energy Differences, and Activation Energies in kcal/mol for the Dissociation Reaction Found in Both Experimental and Computational Works, Including This Work. Values in italics were computed from the equilibrium constants found in each reference.[a]

reaction conditions	T (K)	$K_{CO/HCOOH}$	ΔG	ΔG_a	E_a	ref
gas phase, comput.			4.3[c]		47.1	6
liquid, 0.04−0.16 mol/kg, exp.	443	0.15	*1.67*		34.9	1
liquid, 1.0 M, exp.	573	0.0989[b]	*2.63*			8
liquid, 1.0 M, exp.	548	0.0204[b]	*4.24*			8
liquid, comput.	400		8 ± 2	31 ± 2		this work
gas phase on MgO, comput.			48.9[c]		28.3	15
liquid phase on MgO, comput.	400		42 ± 2	62 ± 2		this work
liquid phase in 0.3 V/Å, comput.	400		24 ± 2	36 ± 2		this work

[a]Molar and molal concentrations refer to those of formic acid. [b]To approximate the equilibrium constant K_{CO} from,[8] we use the percentage decomposition of formic acid after 10 min as reported in the paper, assuming decomposition to CO only. In reality, a small fraction of CO_2 is also detected. [c]Computation at optimized geometries.

along the reaction coordinate, in line with Hammond's postulate.[56,57] Again in line with the latter principle, the electric field lowers both the barrier to synthesis by 10 kcal/mol and the free energy of formic acid by 15 kcal/mol, compared to the bulk water solution in the absence of an electric field. The mineral surface however has a minor effect on the barrier, at the same time strongly stabilizing the product.

Table 1 compares our estimates of free energy differences and barriers with computational and experimental values in the literature, albeit at different temperature. The equilibrium constant for HCOOH decomposition $K_{CO/HCOOH}$ is linked to the reaction free energy by $\Delta G = -RT \ln K_{CO/HCOOH}$ (note the opposite sign of ΔG compared to Figure 6). Values in italic in Table 1 are computed based on this formula. The equilibrium constant varies in the literature depending on the concentration and temperature; however, our computed ΔG appears compatible with the available values to within a few kcal/mol. Especially in the experimental work by Wakai et al.[8] where the concentration is closest to our simulated case, our value is compatible with experimental results and follows qualitatively the trend of increasing ΔG with decreasing temperature. Table 1 reports the activation energies E_a, which in principle are different from the free energy barrier ΔG_a computed in this work. For the reaction at the MgO surface, the only computed energy barrier we found corresponds to the decomposition of an isolated formic acid molecule in a vacuum,[15] hardly comparable to our case. As shown in Figure 2, the electric field and the mineral surface have a similar effect in rendering approximately equiprobable *trans*-HCOOH and $HCOO^-$ (i.e., $pK_a \sim 0$, $\Delta G \sim 0$ in these conditions), with a spontaneous reversible interconversion of the two species on the picosecond time scale (i.e., barrier ∼0). We remark that, on the contrary, in bulk water, the equilibrium between formic acid and the formate ion is experimentally shifted toward formic acid, in agreement with our simulations where the formate ion is never observed. Furthermore, earlier experimental works on the catalytic decomposition of formic acid on metal oxides have consistently shown the formate ion.[10,58] Taken all together, our results indicate that the free energy profiles in Figure 6 are compatible with the available multiple experimental data.

CONCLUSIONS

In summary, our study of the interconversion of carbon monoxide and formic acid at a water−mineral interface shows a significant shift in equilibrium toward formic acid compared to the simulation in bulk water, even though products and reactants remain beyond the first adsorbed water layer, thus never interacting directly with the surface. The effect on the formation barrier is instead relatively small, and as a result decarbonylation at the water−mineral interface is strongly hampered. We posit that the surface electric field at the interface is mostly responsible for this shift, as applying an external electric field on a simulation of the reaction in bulk water has similar qualitative effects, namely, in the structure of the transition states, selection of the trans rotamer, and stabilization of formic acid. Furthermore, both mineral−water interfaces and strong electric fields entail a lowering of the dielectric constant of water, which, in turn, selects the rotamer of formic acid with the lower dipole moment. This work highlights a remarkable property of mineral surfaces beyond traditional catalysis by showing a significant modification of the chemical equilibrium through mere proximity.

ASSOCIATED CONTENT

Supporting Information

The Supporting Information is available free of charge at https://pubs.acs.org/doi/10.1021/acs.jpcc.9b09979.

Explicit details on simulation procedures, the collective variables used, and two-dimensional (2D) free energy landscapes at 300 and 400 K (PDF)

AUTHOR INFORMATION

Corresponding Author

Sara Laporte − *Sorbonne Université, Muséum National d'Histoire Naturelle, UMR CNRS 7590, IMPMC, F-75005 Paris, France; CNR-IOM DEMOCRITOS, SISSA, Trieste 34136, Italy;* orcid.org/0000-0001-5079-5161; Phone: 39 (0)40 3787 443; Email: slaporte@sissa.it

Authors

Fabio Pietrucci − *Sorbonne Université, Muséum National d'Histoire Naturelle, UMR CNRS 7590, IMPMC, F-75005 Paris, France;* orcid.org/0000-0002-4892-2667

François Guyot − *Sorbonne Université, Muséum National d'Histoire Naturelle, UMR CNRS 7590, IMPMC, F-75005 Paris, France; Institut Universitaire de France (IUF), 75005 Paris, France*

A. Marco Saitta − *Sorbonne Université, Muséum National d'Histoire Naturelle, UMR CNRS 7590, IMPMC, F-75005 Paris, France*

https://dx.doi.org/10.1021/acs.jpcc.9b09979
J. Phys. Chem. C 2020, 124, 5125−5131

Complete contact information is available at:
https://pubs.acs.org/10.1021/acs.jpcc.9b09979

Notes

The authors declare no competing financial interest.

■ ACKNOWLEDGMENTS

The authors acknowledge funding from the Ile-de-France Region through the DIM Oxymore and access to the HPC resources of IDRIS.

■ REFERENCES

(1) Yasaka, Y.; Yoshida, K.; Wakai, C.; Matubayasi, N.; Nakahara, M. Kinetic and equilibrium study on formic acid decomposition in relation to the water−gas-shift reaction. *J. Phys. Chem. A* **2006**, *110*, 11082−11090.
(2) Pérez-Fortes, M.; Schóneberger, J. C.; Boulamanti, A.; Harrison, G.; Tzimas, E. Formic acid synthesis using CO2 as raw material: Techno-economic and environmental evaluation and market potential. *Int. J. Hydrogen Energy* **2016**, *41*, 16444−16462. Special issue: hydrogen and fuel cell developments: A special issue on the 8th international conference on sustainable energy and environmental protection (SEEP 2015), August 11−14, 2015, Paisley, Scotland, UK.
(3) Markets and Markets, Formic acid market by types (grades of 85%, 94%, 99%, and others) by application (agriculture, leather & textile, rubber, chemical & pharmaceuticals, & others) & by geography - Global trends, forecasts to 2019. https://www.marketsandmarkets.com/Market-Reports/formic-acid-Market-69868960.html (accessed April 16, 2019).
(4) Pietrucci, F.; Saitta, A. M. Formamide reaction network in gas phase and solution via a unified theoretical approach: Toward a reconciliation of different prebiotic scenarios. *Proc. Natl. Acad. Sci. U.S.A.* **2015**, *112*, 15030−15035.
(5) Yu, J.; Savage, P. E. Decomposition of formic acid under hydrothermal conditions. *Ind. Eng. Chem. Res.* **1998**, *37*, 2−10.
(6) Zhang, Y.; Zhang, J.; Zhao, L.; Sheng, C. Decomposition of formic acid in supercritical water. *Energy Fuels* **2010**, *24*, 95−99.
(7) Maiella, P. G.; Brill, T. B. Spectroscopy of hydrothermal reactions. 10. Evidence of wall effects in decarboxylation kinetics of 1.00 m HCO2X (X = H, Na) at 280-330 °C and 275 bar. *J. Phys. Chem. A* **1998**, *102*, 5886−5891.
(8) Wakai, C.; Yoshida, K.; Tsujino, Y.; Matubayasi, N.; Nakahara, M. Effect of concentration, acid, temperature, and metal on competitive reaction pathways for decarbonylation and decarboxylation of formic acid in hot water. *Chem. Lett.* **2004**, *33*, 572−573.
(9) Yasaka, Y.; Wakai, C.; Matubayasi, N.; Nakahara, M. Controlling the equilibrium of formic acid with hydrogen and carbon dioxide using ionic liquid. *J. Phys. Chem. A* **2010**, *114*, 3510−3515.
(10) Trillo, J. M.; Munuera, G.; Criado, J. M. Catalytic decomposition of formic acid on metal oxides. *Catal. Rev.* **1972**, *7*, 51−86.
(11) Lippens, B.; Webb, A. Formic Acid Synthesis. USUS 3,759,990 1973.
(12) Noto, Y.; Fukuda, K.; Onishi, T.; Tamaru, K. Mechanism of formic acid decomposition over dehydrogenation catalysts. *Trans. Faraday Soc.* **1967**, *63*, 3081−3087.
(13) Peng, X. D.; Barteau, M. A. Dehydration of carboxylic acids on the MgO(100) surface. *Catal. Lett.* **1991**, *7*, 395−402.
(14) Zhao, L.; Lolli, G.; Wolf, A.; Mleczko, L. Closing the gap in formic acid reforming. *Chem. Eng. Technol.* **2018**, *41*, 1631−1638.
(15) Lintuluoto, M.; Nakatsuji, H.; Hada, M.; Kanai, H. Theoretical study of the decomposition of HCOOH on an MgO(100) surface. *Surf. Sci.* **1999**, *429*, 133−142.
(16) Schlaich, A.; Knapp, E. W.; Netz, R. R. Water dielectric effects in planar confinement. *Phys. Rev. Lett.* **2016**, *117*, No. 048001.
(17) Cheng, J.; Sprik, M. The electric double layer at a rutile TiO 2 water interface modelled using density functional theory based molecular dynamics simulation. *J. Phys. Condens. Matter* **2014**, *26*, No. 244108.
(18) Cicero, G.; Grossman, J. C.; Schwegler, E.; Gygi, F.; Galli, G. Water confined in nanotubes and between graphene Sheets: A first principle study. *J. Am. Chem. Soc.* **2008**, *130*, 1871−1878.
(19) Ong, S.; Zhao, X.; Eisenthal, K. B. Polarization of water molecules at a charged interface: second harmonic studies of the silica/water interface. *Chem. Phys. Lett.* **1992**, *191*, 327−335.
(20) Vlcek, L.; Zhang, Z.; Machesky, M. L.; Fenter, P.; Rosenqvist, J.; Wesolowski, D. J.; Anovitz, L. M.; Predota, M.; Cummings, P. T. Electric double layer at metal oxide surfaces: static properties of the cassiterite-water interface. *Langmuir* **2007**, *23*, 4925−4937.
(21) Laporte, S.; Finocchi, F.; Paulatto, L.; Blanchard, M.; Balan, E.; Guyot, F.; Saitta, A. M. Strong electric fields at a prototypical oxide/water interface probed by ab initio molecular dynamics: MgO(001). *Phys. Chem. Chem. Phys.* **2015**, *17*, 20382−20390.
(22) Fried, S. D.; Bagchi, S.; Boxer, S. G. Extreme electric fields power catalysis in the active site of ketosteroid isomerase. *Science* **2014**, *346*, 1510−1514.
(23) Saarenketo, T. Electrical properties of water in clay and silty soils. *J. Appl. Geophys.* **1998**, *40*, 73−88.
(24) Cassone, G.; Giaquinta, P. V.; Saija, F.; Saitta, A. M. Liquid methanol under a static electric field. *J. Chem. Phys.* **2015**, *142*, No. 054502.
(25) Saitta, A. M.; Saija, F. Miller experiments in atomistic computer simulations. *Proc. Natl. Acad. Sci. U.S.A.* **2014**, *111*, 13768−13773.
(26) Saitta, A. M.; Saija, F.; Giaquinta, P. V. Ab Initio Molecular Dynamics Study of Dissociation of Water under an Electric Field. *Phys. Rev. Lett.* **2012**, *108*, No. 207801.
(27) Rothfuss, C. J.; Medvedev, V. K.; Stuve, E. M. The influence of the surface electric field on water ionization: a two step dissociative ionization and desorption mechanism for water ion cluster emission from a platinum field emitter tip. *J. Electroanal. Chem.* **2003**, *554*−*555*, 133−143. Special issue in memory of Professor M. J. Weaver.
(28) Pietrucci, F. Strategies for the exploration of free energy landscapes: unity in diversity and challenges ahead. *Rev. Phys.* **2017**, *2*, 32−45.
(29) Melius, C. F.; Bergan, N. E.; Shepherd, J. E. Effects of water on combustion kinetics at high pressure. *Symp. (Int.) Combust.* **1991**, *23*, 217−223. Twenty-Third Symposium (International) on Combustion, July 22−27, 1990, Orléans, France.
(30) Matubayasi, N.; Nakahara, M. Hydrothermal reactions of formaldehyde and formic acid: Free-energy analysis of equilibrium. *J. Chem. Phys.* **2005**, *122*, No. 074509.
(31) Chen, H.-T.; Chang, J.-G.; Chen, H.-L. A computational study on the decomposition of formic acid catalyzed by (H2O)x, x = 0-3: comparison of the gas-phase and aqueous-phase results. *J. Phys. Chem. A* **2008**, *112*, 8093−8099.
(32) Perdew, J. P.; Burke, K.; Ernzerhof, M. Generalized gradient approximation made simple. *Phys. Rev. Lett.* **1996**, *77*, 3865−3868.
(33) Giannozzi, P.; Baroni, S.; Bonini, N.; Calandra, M.; Car, R.; Cavazzoni, C.; Ceresoli, D.; Chiarotti, G. L.; Cococcioni, M.; Dabo, I. QUANTUM ESPRESSO: a modular and open-source software project for quantum simulations of materials. *J. Phys. Condens. Matter* **2009**, *21*, No. 395502.
(34) Grimme, S. Semiempirical GGA-type density functional constructed with a long-range dispersion correction. *J. Comput. Chem.* **2006**, *27*, 1787−1799.
(35) Car, R.; Parrinello, M. Unified approach for molecular dynamics and density-functional theory. *Phys. Rev. Lett.* **1985**, *55*, 2471−2474.
(36) Resta, R.; Vanderbilt, D. Theory of Polarization: A Modern Approach. In *Physics of Ferroelectrics: A Modern Perspective*; Ahn, C.; Rabe, K.; Triscone, J., Eds.; Springer-Verlag; Chapter 2, 2007.
(37) Bussi, G.; Donadio, D.; Parrinello, M. Canonical sampling through velocity rescaling. *J. Chem. Phys.* **2007**, *126*, No. 014101.
(38) Laio, A.; Parrinello, M. Escaping free-energy minima. *Proc. Natl. Acad. Sci. U.S.A.* **2002**, *99*, 12562−12566.

(39) Kumar, S.; Rosenberg, J. M.; Bouzida, D.; Swendsen, R. H.; Kollman, P. A. The weighted histogram analysis method for free-energy calculations on biomolecules. I. The method. *J. Comput. Chem.* **1992**, *13*, 1011−1021.
(40) Branduardi, D.; Gervasio, F. L.; Parrinello, M. From A to B in free energy space. *J. Chem. Phys.* **2007**, *126*, No. 054103.
(41) Pérez-Villa, A.; Pietrucci, F.; Saitta, A. M. Prebiotic chemistry and origins of life research with atomistic computer simulations. *Phys. Life Rev.* **2018**, DOI: 10.1016/j.plrev.2018.09.004.
(42) Pérez-Villa, A.; Saitta, A. M.; Georgelin, T.; Lambert, J.-F.; Guyot, F.; Maurel, M.-C.; Pietrucci, F. Synthesis of RNA nucleotides in plausible prebiotic conditions from ab initio computer simulations. *J. Phys. Chem. Lett.* **2018**, *9*, 4981−4987.
(43) Cassone, G.; Pietrucci, F.; Saija, F.; Saitta, A. M. *Computational Approaches for Chemistry under Extreme Conditions*; Springer, 2019; pp 95−126.
(44) Kroonblawd, M. P.; Pietrucci, F.; Saitta, A. M.; Goldman, N. Generating converged accurate free energy surfaces for chemical reactions with a force-matched semiempirical Model. *J. Chem. Theory Comput.* **2018**, *14*, 2207−2218.
(45) Pietrucci, F.; Aponte, J. C.; Starr, R. D.; Pérez-Villa, A.; Elsila, J. E.; Dworkin, J. P.; Saitta, A. M. Hydrothermal decomposition of amino acids and origins of prebiotic meteoritic organic compounds. *ACS Earth Space Chem.* **2018**, *2*, 588−598.
(46) Bonomi, M.; Branduardi, D.; Bussi, G.; Camilloni, C.; Provasi, D.; Raiteri, P.; Donadio, D.; Marinelli, F.; Pietrucci, F.; Broglia, R. A.; et al. PLUMED: A portable plugin for free-energy calculations with molecular dynamics. *Comput. Phys. Commun.* **2009**, *180*, 1961−1972.
(47) Marzari, N.; Mostofi, A. A.; Yates, J. R.; Souza, I.; Vanderbilt, D. Maximally localized Wannier functions: Theory and applications. *Rev. Mod. Phys.* **2012**, *84*, 1419−1475.
(48) Scuseria, G. E.; Miller, M. D.; Jensen, F.; Geertsen, J. The dipole moment of carbon monoxide. *J. Chem. Phys.* **1991**, *94*, 6660−6663.
(49) Kim, H.; Keller, R.; Gwinn, W. D. Dipole moment of formic acid, HCOOH and HCOOD. *J. Chem. Phys.* **1962**, *37*, 2748−2750.
(50) Freitas, T. C.; Coutinho, K.; do N. Varella, M. T.; Lima, M. A. P.; Canuto, S.; Bettega, M. H. F. Electron collisions with the HCOOH−(H2O)n complexes (n = 1, 2) in liquid phase: The influence of microsolvation on the π^* resonance of formic acid. *J. Chem. Phys.* **2013**, *138*, No. 174307.
(51) van Erp, T. S.; Meijer, E. J. Ab initio molecular dynamics study of aqueous solvation of ethanol and ethylene. *J. Chem. Phys.* **2003**, *118*, 8831−8840.
(52) Kemp, D. D.; Gordon, M. S. An interpretation of the enhancement of the water dipole moment due to the presence of other water molecules. *J. Phys. Chem. A* **2008**, *112*, 4885−4894.
(53) Hickey, A. L.; Rowley, C. N. Benchmarking quantum chemical methods for the calculation of molecular dipole moments and polarizabilities. *J. Phys. Chem. A* **2014**, *118*, 3678−3687.
(54) Danielewicz-Ferchmin, I.; Ferchmin, A. R. Static permittivity of water revisited: ? in the electric field above 108 V m-1 and in the temperature range 273 ≤ T ≤ 373 K. *Phys. Chem. Chem. Phys.* **2004**, *6*, 1332−1339.
(55) Fumagalli, L.; Esfandiar, A.; Fabregas, R.; Hu, S.; Ares, P.; Janardanan, A.; Yang, Q.; Radha, B.; Taniguchi, T.; Watanabe, K.; et al. Anomalously low dielectric constant of confined water. *Science* **2018**, *360*, 1339−1342.
(56) Hammond, G. S. A correlation of reaction rates. *J. Am. Chem. Soc.* **1955**, *77*, 334−338.
(57) Agmon, N. Quantitative Hammond postulate. *J. Chem. Soc., Faraday Trans. 2* **1978**, *74*, 388−404.
(58) Mars, P.; Scholten, J.; Zwietering, P. The Catalytic Decomposition of Formic Acid. In *Advances in Catalysis*, Eley, D.; Pines, H.; Weisz, P. B., Eds.; Academic Press, 1963; Vol. *14*; pp 35−113.

https://dx.doi.org/10.1021/acs.jpcc.9b09979
J. Phys. Chem. C 2020, 124, 5125−5131